Measurement 198 (2022) 111365

Contents lists available at ScienceDirect

Measurement

journal homepage: www.elsevier.com/locate/measurement

Inexpensive photogrammetry applied to displacement measurement of a gridshell

Juan Ortiz-Sanz, Mariluz Gil-Docampo, Guillermo Bastos *

Agroforestry Engineering Department, University of Santiago de Compostela, Higher Polytechnic School (Lugo), 27002, Spain[1]

ARTICLE INFO

Keywords:
Gridshell
Photogrammetry
Timber
Metric quality
3D model

ABSTRACT

Gridshells are unexploited structures, over which lengths measurement are difficult to do due to their size and complex curvature. To deformation measurement on a timber gridshell beam and on an entire gridshell, we used an affordable photogrammetry system that consisted of a consumer-level camera, a tripod, a mast with a gimbal to elevate the camera, a laptop, and two photogrammetric software: PhotoModeler Scanner and Metashape. The beam was subjected to a bending test, and the gridshell was loaded with 105 kg of dead load per node on its five central nodes. The maximum error in the measurement was 1.26 mm on the beam and 3.45 mm on the gridshell, which corresponded to 0.77 ‰ error relative to the span of the beam and 0.41 ‰ relative to the length of the gridshell. Three-dimensional models obtained through the proposed method serve as dimensional data with a uniform error around the object.

1. Introduction

Gridshells are a well-established design solution for creating curved forms from linear elements; hence, they are highly suitable for industrialization and standardization [1]. Gridshells are lightweight doubly curved structures that cover open spaces by efficiently using sustainable materials, usually timber [2]. Nevertheless, gridshell has not been widely used in popular structural solutions, like sports, industrial or rural buildings. This type of structures only has been generally used in urban works. Their physical principles have been investigated since the 1970 s, and modern mathematical and digital tools have led to renewed interest in them, primarily through form-finding techniques, in which a mechanical simulation is performed to estimate the final gridshell shape under bending loads [3].

Two types of gridshells are distinguished based on the construction method: strained gridshells and unstrained gridshells. For the first, curvature is obtained on site by bending continuous laths, which are usually made of timber. The use of glass fiber-reinforced polymers in gridshells is growing due to their higher elastic modulus and higher limit strain [4]. The second consist of bespoke nodes and members, which are usually made of steel. Curvature is introduced by using curved members or through the nodes [5]. The object of study of this work is a timber strained gridshell.

Over the past twenty years, research on gridshells has focused on methodologies for generating developable grid configurations and calculating their resulting geometry after they are constructed [6]. Currently, numerical form-finding techniques that simulate the physical behavior of the structure are applied [5]. While the theoretical calculation of stresses and deformations of gridshells has been an active field of research [7], this work contributes to the last step in the construction of a gridshell: verification of a finished loaded structure by displacement measurement [8].

To this end, close-range photogrammetry technology can accurately record the information of the measurand in an instant and obtain the point position relationship of the object [9]. Then, it provides a tool for obtaining the three-dimensional displacements at many points on each tested object. A wide range of equipment for engineering test purposes can be used, varying from low cost solutions with consumer grade cameras, conventional light, printed targets and photogrammetric software like Photomodeler [10] or Metashape [11] to complete solutions with up to cameras, light, targets and analysis software commercial packs, like HEXAGON DPA photogrammetry system [12] GOM TRITOP [13] or Linearis 3D [14].

The main elements influencing photogrammetric accuracy are: number of pixels in the image, quality lens, angles, orientation, photo redundancy and targets. The higher number of pixels in the image, the

* Corresponding author at: University of Santiago de Compostela, Higher Polytechnic School, Rúa Benigno Ledo s/n, Lugo, 27002, Spain.
E-mail address: guillermo.bastos@usc.es (G. Bastos).
[1] CIGEO – Civil and Geomatics Research Group

https://doi.org/10.1016/j.measurement.2022.111365
Received 18 November 2021; Received in revised form 15 April 2022; Accepted 16 May 2022
Available online 21 May 2022

better chance of achieving high accuracy. High-quality lens will produce better results. Points and objects that appear only on photographs with very low subtended angles have much lower accuracy than points on photos that are closer to 90 degrees apart. Making sure the camera positions have good spread will provide the best results. Orientation is the location and angle of the camera for each photo. The orientation quality improves as the number of well-positioned points increases and as the points cover a greater percentage of the photograph área. A point's position is usually more accurately computed when it appears on many photographs, it's called photo redundancy. The accuracy of a 3D point is tied to the precision of its locations in the images. This image positioning can be improved by using targets. The highest accuracy is achieved with a high-resolution camera, with strong angles between photos, most photos have good coverage, most points appear on 6 or more photos, and all points are targets [15].

Close-range photogrammetry has proven to be a useful technology for the experimental verification of behavior models of several types of materials [16–19], both in laboratory [20,21], and in situ [9,16,22]. In the particular case of timber, a pioneering research study was conducted in the 1990 s to validate a failure criterion [23]. Currently, close-range photogrammetry is known for providing 3D displacements, strains, stress components, and mechanical properties of timber at many points on each specimen without the need for direct contact [24]. In addition, as timber is considerably less stiff than other materials, low-cost photogrammetry could be applied to timber to evaluate its mechanical properties or carry out validations using the finite element method with high accuracy and little investment [25]. Current photogrammetric technology enables us to obtain geometric data with high precision and reliability, even with nonmetric cameras, using a simple calibration process [26,27]. For example, the cameras in modern cell phones were used to estimate volumes in the mining industry [28] and 3D coordinates of buildings [29].

The present work describes the implementation and evaluation of an affordable close-range photogrammetric system for acquiring the 3D displacements of two wooden structures. The first is a timber composite beam that resembles a gridshell element between nodes. It was subjected to a three-point bending test [30]. The second is a gridshell, which was loaded with dead weights on its central nodes. Both structures were made of *Eucalyptus globulus* strips.

To evaluate the applicability of the proposed photogrammetric technique, dimensional verification was performed between the structures and their generated 3D models. The software that was employed was PhotoModeler Scanner v6 (2008) [31] and, on the gridshell, Agisoft Metashape Professional v1.7.5 (2021) [11]. Both tools demonstrate not only the measurement capabilities of close-range photogrammetry but also the improvement of photogrammetry in the last decade.

2. Analyzed structures

Gridshells are lightweight doubly curved structures that cover open spaces by efficiently using sustainable materials, usually timber [2]. The curvature is formed over initially straight elements, either starting flat on the ground and by pushing upward or assembling the structure above ground and lowering it by its own weight [32]. Single-layer gridshells have a single lath in each direction, while double-layer gridshells have two laths in each direction, which provides greater out-of-plane bending strength and stiffness. These two layers can slide and rotate along each other during assembly such that the flexural stiffness of the members is that of a single layer gridshell [32]. After erecting such a structure, when a double-layered gridshell has reached the final shape, the nodes are tightened, shear blocks of timber are inserted between the layers, and the structure is stiffened by a diagonal bracing system. A double-layer gridshell with a gap between the layers that is equal to the thickness of the members has a flexural stiffness of 26 times that of a single layer [2].

The first analyzed structure was a wooden component of a double-layered gridshell. It consisted of two strips that were joined at the ends with shear blocks and bolts. The second structure was a gridshell. 3D photogrammetry was applied to displacement measurement of these structures. While the beam corresponded to a double-layered gridshell, we applied photogrammetry to a single-layered gridshell to obtain larger displacements and, thus, to produce larger absolute errors at measurement results. The construction process of this prototype is presented in [33], which includes numerical modeling, a novel erection method, stress tests on beams and joints, and displacement measurement in the loaded structure using the procedure that is described in the present work. The dimensions of both structures are presented in Fig. 1.

3. Materials

The basic equipment that was employed included a 3-point bending tester with load and displacement control and a consumer-grade Canon Eos 550D camera with a CMOS sensor of 18 megapixels with dimensions of 22.3 mm × 14.9 mm and pixel size of 4.3 μm × 4.3 μm. This camera was used in conjunction with a Canon EF 20 mm 1:2,8 (Canon Inc., Ota, Tokyo, Japan). Through the camera-specific software EOS Utility Ink, a laptop instantly received the video signal from the camera through a conventional USB cable, which also enabled modification of the camera parameters and triggering.

The photogrammetric software PhotoModeler Scanner (PS) v6 (2008) [31] and Metashape v1.7.5 (2021) [11] were used to process the photographs and generate 3D models of the structures. The work in spreadsheets was conducted with the open-source software LibreOffice Calc 4.2 [34]. The drawings were constructed with the open-source software QCAD [35].

We used coded- and dot-type targets that PS generated, as shown in Fig. 2. Coded targets support the determination of corresponding points in the image matching that the photogrammetric software performs, and they improve the accuracy and precision of feature recognition [36,37]. They are mandatory in PS: First, the targets are recognized and placed together in 3D space with their coordinates. Second, PS uses the coordinates of the targets to orient the photos and to build a 3D point cloud of the photographed object. Targets are a complementary aid in Metashape.

A caliper was used to verify the precision at printing of the coded targets. A 5 m-long steel Class II tape measure [38] was used to assess the metric quality of the 3D model. To move and trigger the camera, an elevator device was applied, which comprised two parts: a lift telescopic mast and a camera gimbal. The mast was a commercial manually extendible device that was constructed of lightweight materials (aluminum and plastic). The working length of the mast was set at 5 m. The gimbal, which was mounted at the end of the mast, was made by us with an aluminum profile, and it enabled us to modify the angle between the optical axis and the floor plane. One person handled the mast and the orientation of the camera, while another person triggered the camera from a computer. The total investment in photogrammetric equipment—camera, lens, software (PS), tripod and mast—was approximately 4,000 € ($4,660). A lifetime license with limited updating currently costs $3,500 for Metashape Professional and $2,995 for PhotoModeler Premium, which is the product that replaced PS. In addition, the loading of the gridshell was performed using ten 50 L water drums.

4. Methodology

The method that was followed is essentially as follows:

1st: Camera calibration

The inner orientation of the optical elements is necessary for resolving the parameters of the camera, and it was obtained using the calibration module of the software. To be able to carry it out, some photos were taken on a calibration sheet printed on a simple consumer-grade printer. These photos were imported by the software and the internal parameters of the camera were automatically determined. The

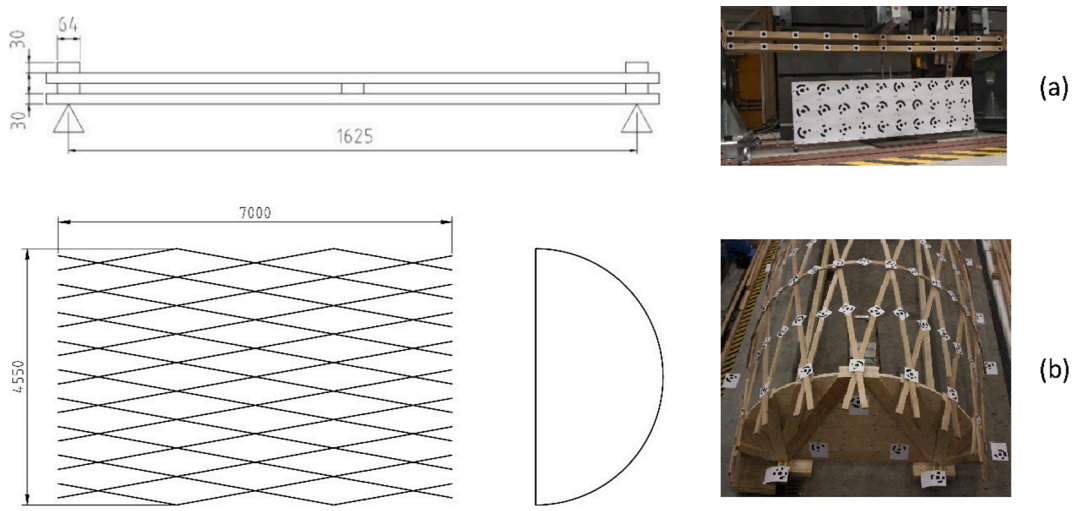

Fig. 1. Dimensions (mm) of the gridshell beam (a) and the gridshell (b).

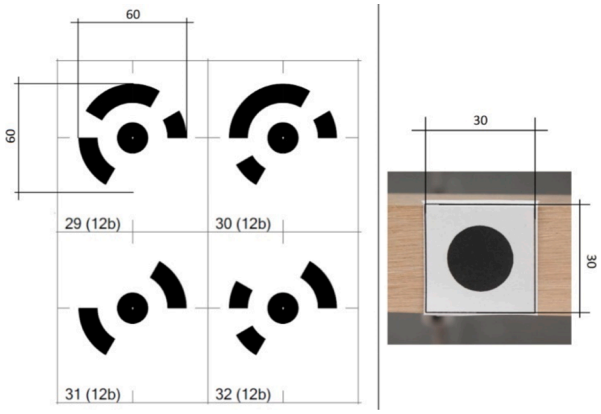

Fig. 2. Coded targets.

parameters of calibration were filed and the software used them, with the camera so adjusted, in next projects. The camera calibration is the most important step in the entire 3D modelling process, because it underpins the accuracy achievable by the photogrammetric process and performance [39].

2nd: Design and setup of the image acquisition

The design of the photographic acquisition began with the visual inspection of the testing environment for both structures. Next, we decided on the place from which the photographs were to be taken, the photographing distance, and the configuration of the camera settings (ISO, shutter speed and the lens aperture).

The software attempted to recognize the coded targets in the photos. In PS, the identification of a target in several photographs enabled the construction of an elementary 3D model that consisted only of the targeted points in the space. It helped orient the cameras, namely, determine the position and orientation of the camera when triggered for each photo. Once the cameras were oriented, a more "solid" 3D model could be created by generating a dense point cloud, followed by a meshed model and a textured model, over which distance measurement could be done. In Metashape, the recognition of coded targets boosted the determination of matched points between images, which were used to build the 3D model.

To provide data redundancy to the software, the number of coded targets that were used was higher than the minimum required. To facilitate target recognition by the software, the coded targets were sized larger than the minimum size. This was expected to lead to a more reliable 3D model. The final 3D model is more reliable because of the redundancy of the coded targets, which allowed the used software to apply adjustment observations techniques.

The position where the targets were placed also had to be carefully planned. Some of the targets were model-control points; they were employed to provide data redundancy and to scale, translate and rotate the generated 3D model. For each project, the points that were located by three coded targets were used to translate and rotate the 3D model to bring all the points to a unique coordinate system for all load steps. Two model-control points were employed to scale the model.

The other targets were the dimensional-checking points, which were employed to evaluate the geometric quality of the model, namely, the precision of the distances between the 3D coordinates in the model compared to those in the real structure.

3rd: Image acquisition

The composite beam was photographed during three load steps, while the gridshell was photographed unloaded under the maximum load. We monitored general deformation but under static load, then, only one camera can be used. Data redundancy was also important in relation to the number of photos, without reaching a number that requires an excessive computer-processing time. The laboratory had diffuse light during the daytime, which was required to obtain photographs with homogeneous gloss and color conditions across the object surface.

4th: Photogrammetric processing and evaluation of the geometric quality of the model

The acquired photographs were input into the software. For each structure, after calibrating the cameras, the recognition of coded targets was executed. Next, the photos were oriented, and the 3D model was generated and scaled. To evaluate the accuracy of the generated 3D model measurement results, a series of lengths between checking points were measured in the 3D model. The same distances were measured using a flexometer or a calliper. The error for each measure was determined, and the basic statistical parameters were derived.

Dimensional-checking points were selected on static elements: the coded targets on the vertical panel below the beam and a group of coded targets on the ground around the gridshell. We hypothesize that the measure errors on the static points are very close to the errors on the points that were displaced under the load. This is an advantage of photogrammetry, because accuracy and precision levels of each project can be known through an analysis of errors in static check points, besides, two projects made with the same camera, lens, angles, orientation, photo redundancy and targets will both have similar accuracy and precision. The precision would be proportional to the distance between the target and a laser measurement instrument. In contrast, photograph

overlap due to photoredundancy leads to homogeneous precision along the object surface in photogrammetry. This was observed in the gridshell study. In the case of the beam, the static and nonstatic targeted points were close to each other and in the same plane.

The 1st step was common to both structures. Below, the actions that were taken for each structure in Steps 2 to 4 are summarized.

4.1. Photogrammetric procedure on the gridshell beam

The camera on a tripod was shot from seven positions. The averaged distance between the camera and the middle point of the beam was 1.35 m. For the described model-control points and dimensional-checking points, we used coded targets of 12 bits with 60 mm diameter. They were printed on a 100 mm-spaced grid and placed on a panel, which stayed static during the test. To test the target recognition on the beam, we used dot-type targets of 30 mm diameter that were 151 mm-spaced along the beam. Eleven pairs were laid on the beam, one of them at the middle point, and an additional pair on each beam end. These details are presented in Fig. 3. We had a total of 26 points on the beam and 30 points on the static panel.

Once the coded targets were placed, the panel with the targets was leveled with a plumb. After initiating the bending test, the structure was photographed from the seven locations in three load steps (see Fig. 4): The first load step was the idle stage, which was the reference stage when determining the displacements under load; the second load step was the intermediate time between the idle state and the beam breaking; and the third load step corresponds to the immediate moment before breaking, namely, under the maximum load. The targets had to be static while being photographed; thus, the test was paused in each load step. If this were not possible, photogrammetry could also be applied by using at least three synchronized cameras. Seven photos were acquired in each load step.

Three of the model-control points of the panel were used to scale the 3D model and to place the (x, y, z) coordinate system. The dimensional quality of the model was evaluated through the errors in four distances between eight checking points of the panel. Real length measurement were done on the panel with a caliper or a flexometer. The relative error was provided in relation to the beam length, namely, 1625 mm.

4.2. Photogrammetric procedure on the gridshell

We attached gridshell coded targets of 14 bits and 150 mm diameter. Five model-control points and ten dimensional-checking points were placed on the ground. The gridshell was photographed in two load cases: unloaded and under the maximum load, namely, 105 kg dead load that was suspended from each of the five central nodes, as shown in Fig. 5-b.

The gridshell was photographed along two trajectories that surrounded it. In the first trajectory, the operator photographed the structure while walking around. In the second trajectory, the camera was inserted in a gimbal on the top of the mast. Two representative images are presented in Fig. 5. The number of captured photos from the ground and with the mast were 112 and 53, respectively, with no load and 52 and 41, respectively, over the loaded step. The (minimum) camera-object distance remained close to 3.3–3.5 m from the mast, 1.6–1.9 m from the ground on long sides and 3.4–3.7 m on short sides.

Two of the five model-control points were used to scale the 3D model and the other three ones were used to place the (x, y, z) coordinate system. The geometric quality of the obtained 3D model was evaluated through 5 distances between the ten dimensional-checking points that were chosen in the gridshell scene. The reference distance measurement were done on the structure with a flexometer. As can be appreciated in Fig. 6, each measure where carefully obtained with a camera. The relative error was provided in relation to the length of the diagonal of the rectangular base, namely, 8348.8 mm.

5. Practical cases and results

Results of both experiments will be described in this section. Time required, main difficulties and measures quality will be exposed for each one.

5.1. Gridshell beam

The planning of the test with the photographic sessions took 16 h. It was a simpler task than the gridshell case, not only due to the smaller size of the beam but also because the test is prescribed by [30]. To carry out the photographing session, a tripod was used, and the bending test was paused in the second and third load steps. This enabled photography at a low shutter speed (2 s), and we could optimize the images that were captured with an ISO-100 and a lens aperture of f/11. The total photographing work took 30 min.

The processing of the images and distance measurement on the 3D model for each load step took 8 h. It was composed of the introduction of input variables, corrections of errors in the images, study of the errors in

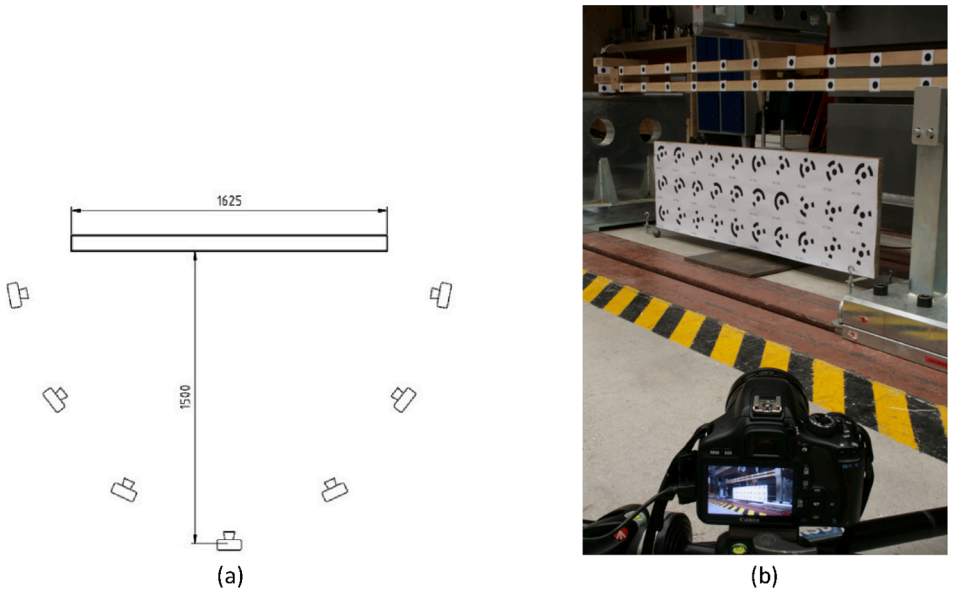

Fig. 3. Scene of the bending test on the beam: (a) Camera locations and (b) an overview of the scene.

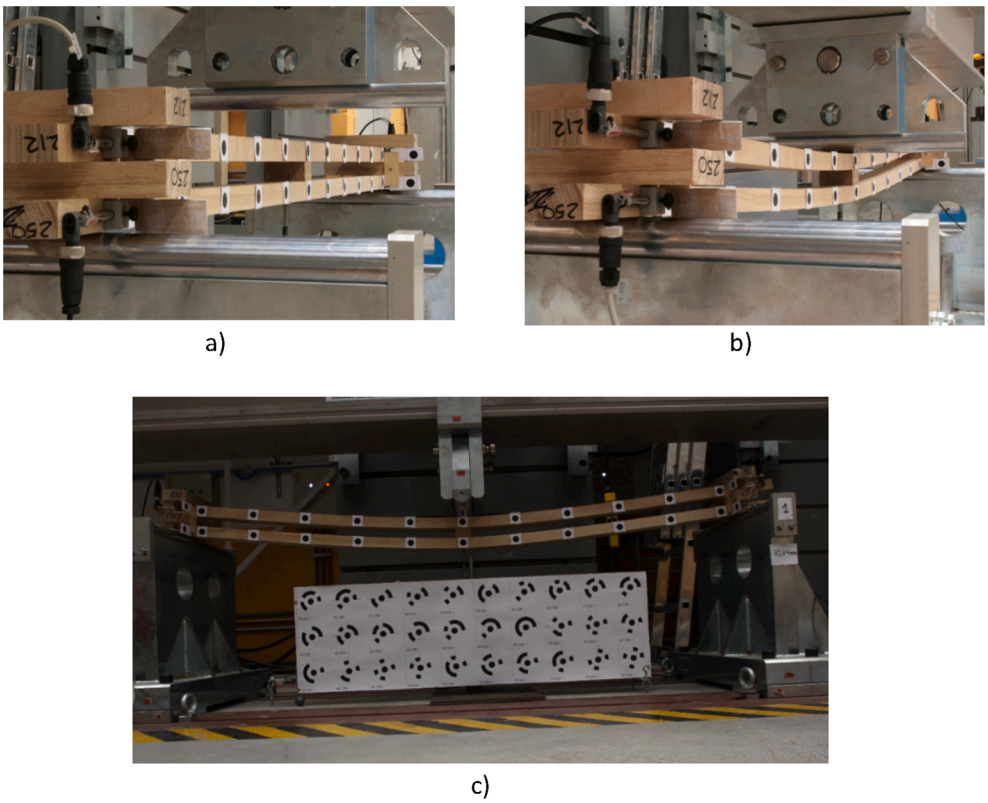

Fig. 4. Photographed load status: (a) No load, (b) half-time between loading start and failure, and (c) maximum load before failure.

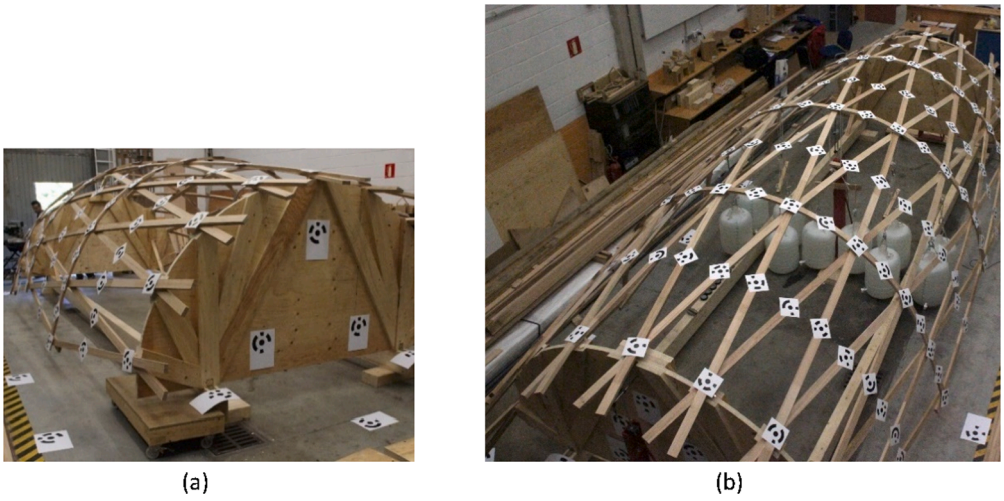

Fig. 5. Two photographing heights: (a) Standing on the floor and (b) from the mast.

the targets, refinement of the obtained 3D model, orientation and scaling of the 3D model, and gathering of the (x, y, z) coordinates of the points of the 3D model. All of the photographs were correctly processed, and the targets were correctly recognized, as shown in Fig. 7.

The quality of the 3D model in PS was evaluated based on the 4 distances between the checking points of the panel. The fundamental statistical parameters are collected in Table 1.

5.2. Gridshell

The planning of the photogrammetric network took 4 days. The structure stood on the laboratory floor, and the camera was used on the ground and mounted on the mast. Under these conditions, high shutter speed (1/320 s) and ISO (6,400) were required, with a lens aperture of f/5.6, which ensured mostly targets in the scene appeared acceptably in focus. Each photography session required 10 min to be completed.

Once the photographs were acquired, they were imported into PS. After calibrating the camera, the routine for recognizing the coded targets was run, and the photos were processed based on these targets. The same process was performed in Metashape. Representations of the oriented photographs and the targeted points are shown in Fig. 8.

Some of the coded targets were incorrectly recognized in PS: some of them were false-positives that were created on features that were not targets, while others were placed on the rings of targets instead of in their center circles. An example of each error is presented in Fig. 9. We deleted the false-positives and corrected the ring-type detections. We

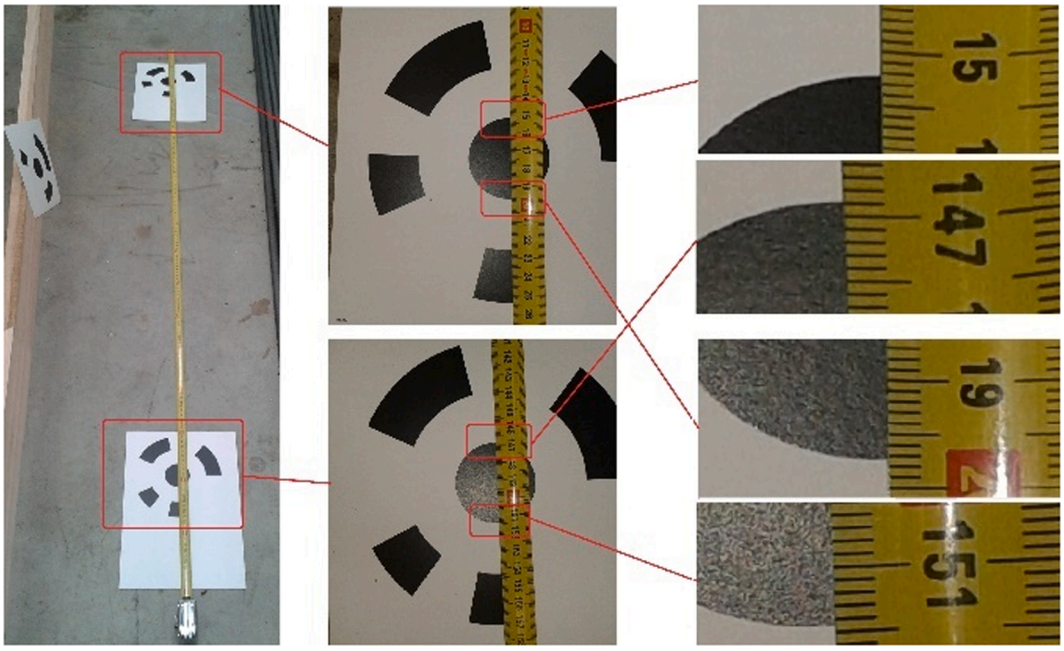

Fig. 6. Distance measurement between 305 and 306 coded targets.

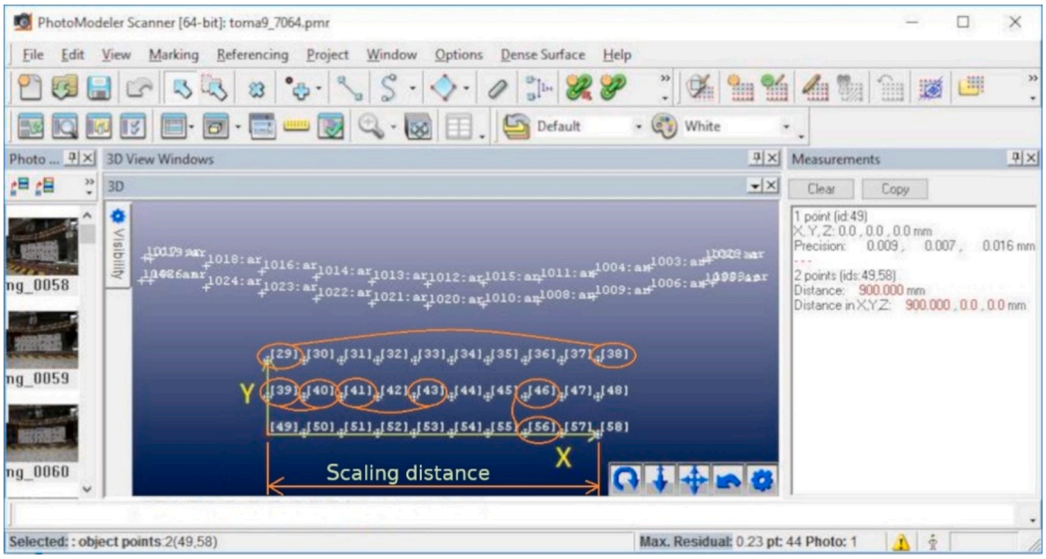

Fig. 7. Model-control points and dimensional-checking points on the static panel.

Table 1
Metric evaluation on the gridshell beam.

	Pair of targets	29, 38	56, 46	39, 40	41, 43	Mean value (mm)	Standard deviation (mm)
	Ground truth (mm)	900	100	100	200		
Load step 1	Measures on the 3D model (mm)	900.13	98.74	99.66	200.22		
	Absolute error (mm)	0.13	1.26	0.34	0.22	0.49	0.52
	Relative error (‰)	0.08	0.77	0.21	0.14		
Load step 2	Measures on the 3D model (mm)	900.07	98.76	99.67	200.24		
	Absolute error (mm)	0.072	1.24	0.33	0.24	0.47	0.52
	Relative error (‰)	0.04	0.76	0.20	0.24		
Load step 3	Measures on the 3D model (mm)	900.04	98.77	99.70	200.25		
	Absolute error (mm)	0.042	1.23	0.30	0.25	0.46	0.53
	Relative error (‰)	0.03	0.76	0.19	0.16		

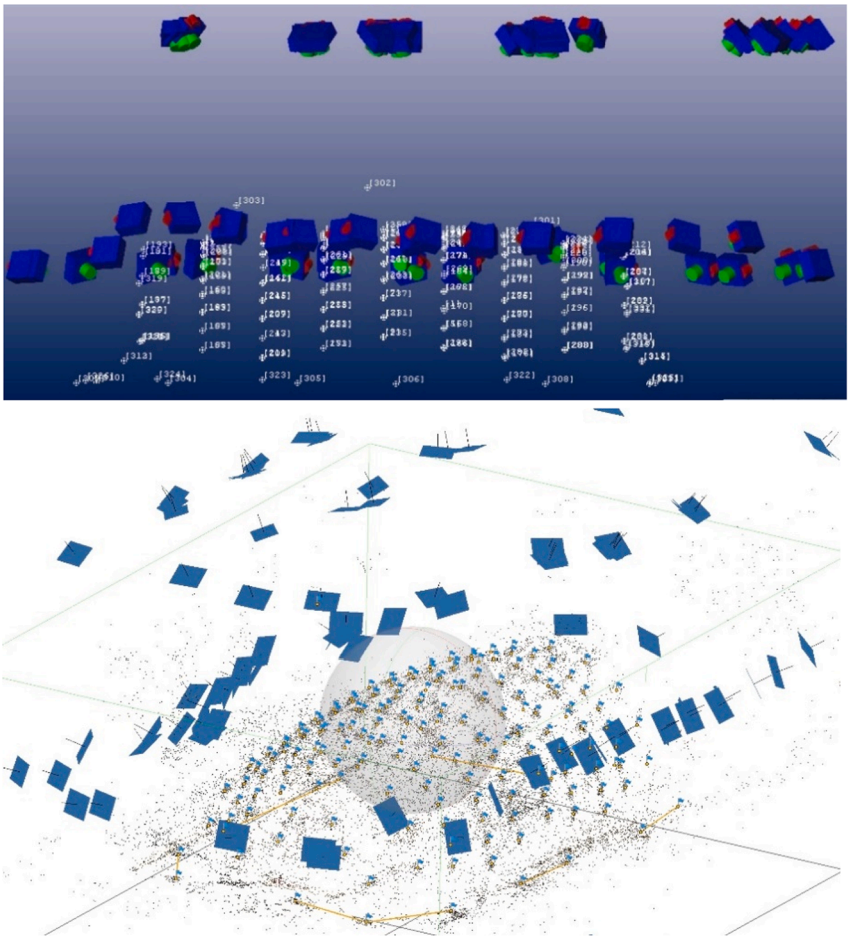

Fig. 8. Positions of the cameras and of the coded targets: (a) PS and (b) Metashape.

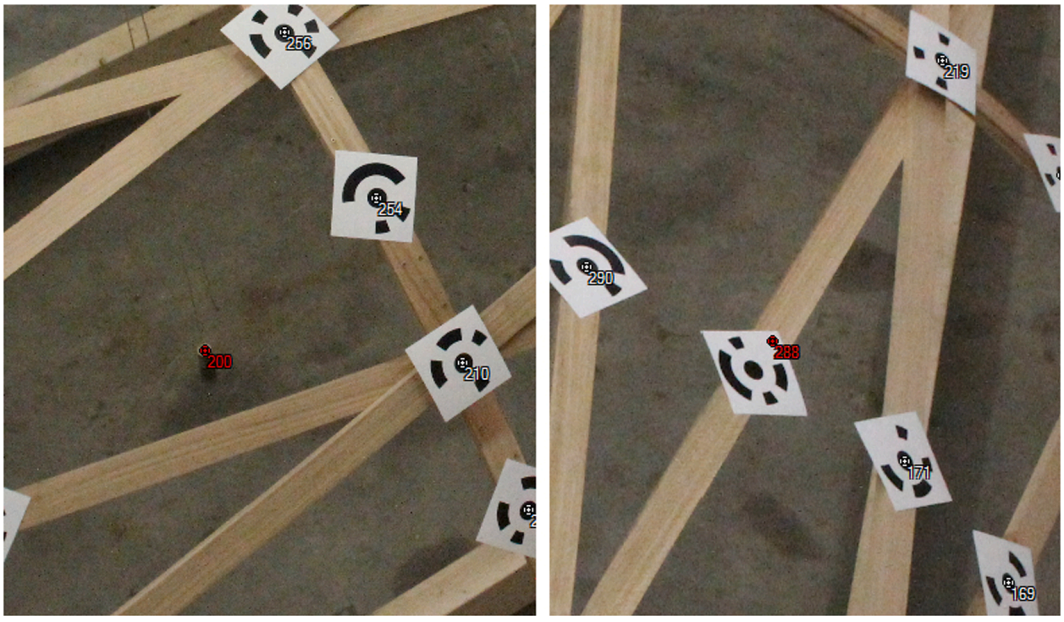

Fig. 9. Target capture by the photogrammetric software.

found that if these amendments were omitted, the metric precision of the model would significantly decrease. PS provides a tool for quickly correcting ring-type detections: only the target is selected within a rectangle, and the recognition is repeated only on that piece of the image. Thus, all of these modifications took little time. Then, distance measurement could be carried out. The processing time of the images was 8 h for each load step. No correction of target recognition was needed in Metashape.

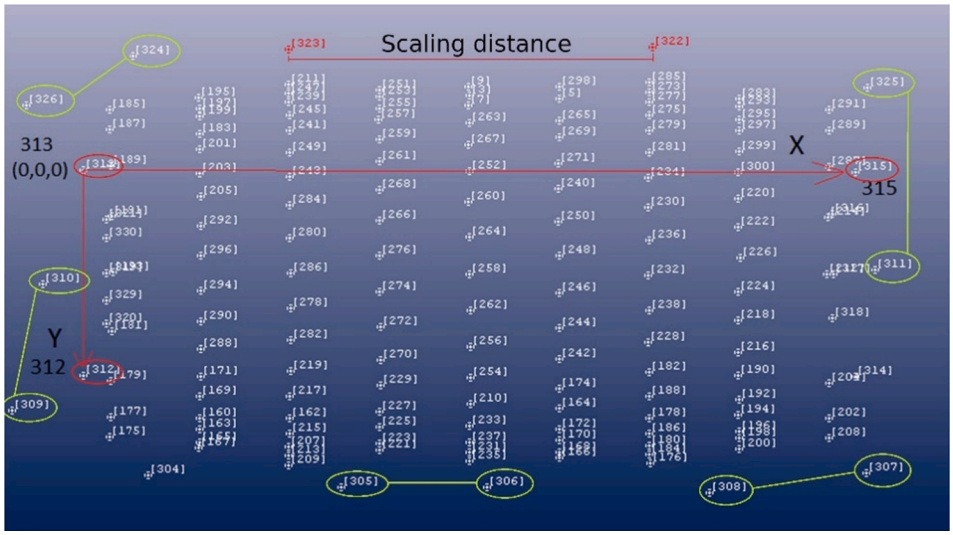

Fig. 10. Points that were used to scale the gridshell model, to place the coordinate system, and to evaluate the metric quality.

Table 2
Analysis of the errors in the measures on the gridshell under no load.

			PhotoModeler Scanner			Metashape			
Pair of targets	Ground truth (mm)	Distance (mm)	Error (mm)	Error abs (mm)	Error (‰)	Distance (mm)	Error (mm)	Error abs (mm)	Error (‰)
309, 310	1166.5	1168.22	1.72	1.72	0.21	1166.92	0.417	0.417	0.050
324, 326	1060	1060.96	0.96	0.96	0.11	1059.26	−0.739	0.739	−0.089
311, 325	1638	1639.94	1.94	1.94	0.23	1638.22	0.222	0.222	0.027
307, 308	1415	1416.48	1.48	1.48	0.18	1415.71	0.71	0.71	0.085
305, 306	1317	1317.93	0.93	0.93	0.11	1316.37	−0.63	0.63	−0.075
Mean value (mm)			1.41	1.41			0,00	0.54	
Standard deviation (mm)			0.45	0.45			0,58	0.22	

Table 3
Analysis of the errors in the measures on the gridshell under the maximum load.

			PhotoModeler Scanner			Metashape			
Pair of targets	Ground truth (mm)	Distance (mm)	Error (mm)	Error abs (mm)	Error (‰)	Distance (mm)	Error (mm)	Error abs (mm)	Error (‰)
309, 310	1166.5	1168.3	1.8	1.8	0.22	1163.95	−2.55	2.55	−0.31
324, 326	1060	1061.53	1.53	1.53	0.18	1058.82	−1.18	1.18	−0.14
311, 325	1638	1640.43	2.43	2.43	0.29	1641.45	3.45	3.45	0.41
307, 308	1415	1416.41	1.41	1.41	0.17	1413.01	−1.99	1.99	−0.24
305, 306	1317	1317.99	0.99	0.99	0.12	1316.25	−0.75	0.75	−0.09
Mean value (mm)			1.63	1.63			0,60	1.98	
Standard deviation (mm)			0.48	0.48			2,12	1.08	

The 5-dimensional checking distances are displayed in Fig. 10. The results of comparing the measures on the model and the real distances are presented in Table 2 and Table 3 for the unloaded case and the loaded case, respectively.

6. Discussion of results

The tasks from both photogrammetry projects could be performed with good coordination with the other tasks, e.g., the setup of the bending test on the beam and the construction of the gridshell. These activities were not even interrupted to place the coded targets. The camera operator only had to check that nobody was standing between the camera and the structure.

The mast was a satisfactory tool for designing an adequate photogrammetric network around the gridshell in the laboratory. All the surfaces of the structure were captured by a camera. The great interest in photogrammetry using unmanned aerial vehicles (UAVs) [40] includes, to a lesser extent, indoor environments [41,42]. However, simple tools such as the mast with a gimbal are more cost-effective than more advanced technologies and safer than ladders or elevating platforms such as basket cranes or bridge crane baskets.

Despite the high quantity of the photographs that were acquired and processed from each scene, the computing time did not exceed 1 day for either the timber beam or the gridshell. Thus, high data redundancy was achieved regarding image processing.

With regard to the beam, as presented in Table 1, the maximum error values did not reach 1.5 mm; hence, the errors were sufficiently small to validate the dimensional quality of the model for structures of this size. The maximum error value was attained in the 1st step, with no load. It corresponds to 0.77 ‰ error in relation to the span of the beam.

In view of these results on the gridshell (Table 2), the magnitudes of the errors could also validate the 3D model that was obtained by

photogrammetry, although the reliability of the obtained models will depend on the noise tolerance of the algorithms used to characterize structural parameters [43]. The maximum error under the maximum load reached 2.43 mm for PS and 3.45 mm for Metashape. Considering the 5 evaluated distances, the mean value and the standard deviation of the absolute errors were lower in PS than in Metashape in the loaded case. We expected Metashape to outperform PS overall, due not to the current difference between the two programs but to the long-time span between their release dates, namely, 13 years. In that time span, commercial photogrammetric software evolved substantially. The better results in PS in the loaded case could be related to the requirement only for the generation of 3D points based on coded targets, not meshed 3D modeling.

7. Conclusions

The deformation measurement on a wooden gridshell beam and on an entire gridshell was done on a 3D model that was generated through photogrammetry. The beam was subjected to a bending test, while the gridshell was loaded on its five central nodes. A photogrammetric network was designed around each structure for three and two load steps for the beam and the gridshell, respectively. Although UAVs are becoming a popular tool in the application of remote sensing to large structures, a mast with a gimbal on the top for placing the camera was an excellent and inexpensive solution and was more agile to operate compared to UAVs. Apart from the cost, the mast has the advantage of being safer than alternative elevating devices, such as basket cranes, ladders, and bridge crane baskets. In addition, among all of these alternatives, only the mast can place the camera through narrow spaces.

The information that was contained in the generated 3D models, together with the locations of singular points (through coded targets), enabled us to estimate the direction and magnitude of the deformations with an admissible error. In the case of the gridshell beam, wich was monitored with PS, an average absolute error that ranged from 0.46 to 0.49 mm was reached, with a standard deviation of 0.52 to 0.53 mm. In the case of the entire gridshell, wich was monitored with PS and Metashape, the measurement results on the PS model resulted in average absolute errors of 1.41 mm and 1.63 mm for the unloaded and loaded cases, respectively, with standard deviations of 0.22 mm and 1.08 mm. The corresponding values in Metashape were 0.54 mm and 1.98 mm for the mean value and 0.22 and 1.08 for the standard deviation.

In view of these results, we concluded that this affordable photogrammetry system enabled us to validate the 3D models of the structures, with verification of the numeric model of the structural design process. The work took a reasonable amount of time: 3 days for the beam and 5 days for the gridshell. Moreover, our tasks did not interrupt the construction of the gridshell. There were no significant differences between PS and Metashape in their accuracy and precision, although photo plan was made without taking into account Metashape requirements. Nevertheless, automatic image processing with Metashape is more effective and quicker than PS, so, that one will be more economical than this one.

These results were obtained with inexpensive close-range photogrammetry. Its cost-effectiveness is one of the reasons for the increasing use of this technology in situ, together with the progress in terms of the camera performance, the elevating tools, the remote control of the camera, and the computing performance and the increasing features of open-source photogrammetric software. Photogrammetry provided a method for deformation measurement on a structure with a uniform error around its surface by virtue of photographic redundancy and overlap, although algorithms used to estimate structural parameters must be designed to work with noise levels compatibles with proposed methodology.

CRediT authorship contribution statement

Juan Ortiz-Sanz: Conceptualization, Data curation, Investigation, Methodology, Software. **Mariluz Gil-Docampo:** Funding acquisition, Writing – original draft, Formal analysis, Supervision. **Guillermo Bastos:** Writing – review & editing, Software, Visualization, Validation.

Declaration of Competing Interest

The authors declare that they have no known competing financial interests or personal relationships that could have appeared to influence the work reported in this paper.

Acknowledgements

The present work was developed in the framework of the research project “Ecological cellular structural systems for a building model for climate change mitigation and forest value enhancement” (Eco-TimberCell) (2017-PI177) Ref.LIFE17 CCM/ES/000074. In addition, it is linked to the Aids for consolidation and structuring of competitive research units in the universities of the Galician University System Ref. ED431B 2020/25. We thank María José Rodríguez González for her collaboration in the tasks of the study. This work was also made possible due to the Spanish State Research Agency (*AEI*), since Dr. Bastos was contracted in the framework of the postdoctoral grant Juan de la Cierva – Formación (FJC2019-039743-I/AEI/10.13039/501100011033).

References

[1] R. Harris, M. Dickson, O. Kelly, The use of timber gridshells for long span structures, in: 8th Int. Conf. Timber Eng., Lahti, Finland, 14–17 June, 2004.
[2] M. Collins, T. Cosgrove, A review of the state of the art of timber gridshell design and construction, in: Civ. Eng. Res. Irel. 2016 (CERI 2016), Galway, Ireland, 29 – 30 August, 2016.
[3] N. Williams, S. Bohnenberger, J. Cherrey, A system for collaborative design on timber gridshells, in: 19th Int. Conf. Comput. Archit. Des. Res. Asia (CAADRIA 2014), The Association for Computer-Aided Architectural Design Research in Asia, Kyoto, Japan, 2014.
[4] S. Xiang, B. Cheng, L.e. Zou, S. Kookalani, An integrated approach of form finding and construction simulation for glass fiber-reinforced polymer elastic gridshells, Struct. Des. Tall Spec. Build. 29 (5) (2020), https://doi.org/10.1002/tal.v29.510.1002/tal.1698.
[5] J. Rombouts, G. Lombaert, L. De Laet, M. Schevenels, A novel shape optimization approach for strained gridshells: Design and construction of a simply supported gridshell, Eng. Struct. 192 (2019) 166–180, https://doi.org/10.1016/j.engstruct.2019.04.101.
[6] E.L. Hernández, C. Gengnagel, S. Sechelmann, T. Rörig, On the materiality and structural behaviour of highly-elastic gridshell structures, in: C. Gengnagel, A. Kilian, N. Palz, F. Scheurer (Eds.), Comput. Des. Model., Springer Berlin Heidelberg, Berlin, Heidelberg, 2011: pp. 123–135. https://doi.org/10.1007/978-3-642-23435-4_15.
[7] C. Adriaenssens, S., Block, P., Veenendaal, D., & Williams, ed., Shell structures for architecture: Form finding and optimization, Routledge, 2014. https://doi.org/10.4324/9781315849270.
[8] JCGM 200 - International vocabulary of metrology, International vocabulary of metrology – Basic and general concepts and associated terms (VIM). 3rd edition. 2008 version with minor corrections, (2008). https://www.bipm.org/documents/20126/2071204/JCGM_200_2012.pdf/f0e1ad45-d337-bbeb-53a6-15fe649d0ff1?version=1.15&t=1641292389029&download=true.
[9] J. Hu, E. Liu, J. Yu, S.-B. Tsai, Application of structural deformation monitoring based on close-range photogrammetry technology, Adv. Civ. Eng. 2021 (2021) 1–11, https://doi.org/10.1155/2021/6621440.
[10] Photomodeler technologies, Photomodeler. Vancouver BC, Canada, (2022). https://www.photomodeler.com/products (accessed April 14, 2022).
[11] Agisoft LLC, Agisoft Metashape, (2021). https://www.agisoft.com/ (accessed July 2, 2021).
[12] Hexagon AB, Photogrammetry. Stockholm, Sweden, (2022). https://www.hexagonmi.com/products/photogrammetry (accessed April 13, 2022).
[13] Carl Zeiss GOM Metrology GmbH, TRITOP. Braunschweig, Germany, (2022). https://www.gom.com/en/products/3d-scanning/tritop (accessed April 12, 2022).
[14] Linearis3D GmbH & Co.KG, LINEARIS3D. Braunschweig, Germany, (2022). http://www.linearis3d.com (accessed April 12, 2022).
[15] PhotoModeler Technologies, Factors affecting accuracy in photogrammetry. Vancouver BC, Canada, (2022). https://www.photomodeler.com/kb/factors_affecting_accuracy_in_photogramm/ (accessed April 6, 2022).

[16] M. Scaioni, L. Barazzetti, A. Giussani, M. Previtali, F. Roncoroni, M.I. Alba, Photogrammetric techniques for monitoring tunnel deformation, Earth Sci. Informatics. 7 (2) (2014) 83–95, https://doi.org/10.1007/s12145-014-0152-8.
[17] X. Zhao, Q. Li, A review on measurement technology for structural testing in civil engineering, Xi'an Jianzhu Keji Daxue Xuebao/Journal Xi'an Univ, Archit. Technol. 49 (2017) 48–55. https://doi.org/10.15986/j.1006-7930.2017.01.008.
[18] A. Mohamed, Y.u. Deng, H. Zhang, S.H.F. Wong, K. Uheida, Y.X. Zhang, M.-C. Zhu, M. Lehmann, Y. Quan, Photogrammetric evaluation of shear modulus of glulam timber using torsion test method and dual stereo vision system, Eur. J. Wood Wood Prod. 79 (5) (2021) 1209–1223, https://doi.org/10.1007/s00107-021-01729-8.
[19] K. Uheida, Y.u. Deng, H. Zhang, L. Galuppi, J. Gao, L.i. Xie, S. Huang, X. Qin, S.H. F. Wong, J. Guo, G. Zhang, A. Mohamed, Determining equivalent-sectional shear modulus in torsion tests for laminated glass beams using photogrammetry method, Compos. Struct. 276 (2021) 114572, https://doi.org/10.1016/j.compstruct.2021.114572.
[20] Z.B. K. Pavelka, J. Šedina, Use of close range photogrammetry for structure parts deformation monitoring, in: Int. Conf. Eng. Sci. Technol., Tatranská Štrba, Slovak Republic, 2015.
[21] I. Detchev, A. Habib, M. El-Badry, Case study of beam deformation monitoring using conventional close range photogrammetry, in: ASPRS 2011 Annu. Conf., Milwaukee, WI, USA, 2011.
[22] H.-G. Maas, U. Hampel, Photogrammetric Techniques in Civil Engineering Material Testing and Structure Monitoring, photogramm eng remote sensing 72 (1) (2006) 39–45.
[23] M. Masuda, A. Iwabuchi, K. Murata, Analyses of fracture criteria using image correlation method, in: L. Boström (Ed.), First RILEM Symp. Timber Eng., RILEM Publications SARL, 1999: pp. 151 – 160.
[24] J. Armesto, I. Lubowiecka, C. Ordóñez, F.I. Rial, FEM modeling of structures based on close range digital photogrammetry, Autom. Constr. 18 (5) (2009) 559–569, https://doi.org/10.1016/j.autcon.2008.11.006.
[25] P. Guindos, J. Ortiz, The utility of low-cost photogrammetry for stiffness analysis and finite-element validation of wood with knots in bending, Biosyst. Eng. 114 (2) (2013) 86–96, https://doi.org/10.1016/j.biosystemseng.2012.11.002.
[26] J. Mills, D. Barber, Geomatics techniques for structural surveying, J. Surv. Eng. 130 (2) (2004) 56–64, https://doi.org/10.1061/(ASCE)0733-9453(2004)130:2(56).
[27] L.M. Honório, M.F. Pinto, M.J. Hillesheim, F.C. de Araújo, A.B. Santos, D. Soares, Photogrammetric process to monitor stress fields inside structural systems, Sensors. 21 (12) (2021) 4023, https://doi.org/10.3390/s21124023.
[28] S. Abbaszadeh, H. Rastiveis, A comparison of close-range photogrammetry using a non-professional camera with field surveying for volume estimation, Int. Arch. Photogramm. Remote Sens. Spat. Inf. Sci. XLII-4/W4 (2017) 1–4, https://doi.org/10.5194/isprs-archives-XLII-4-W4-1-2017.
[29] B.A. Akinade, Investigation of the accuracy of photogrammetric point determination using amateur/non-metric cameras, World Sci. News. 145 (2020) 298–312. http://yadda.icm.edu.pl/yadda/element/bwmeta1.element.psjd-c06c1b48-eaae-4cb8-8cb7-97b0ba4117a9.
[30] Asociación Española de Normalización y Certificación (AENOR), UNE-EN 408: 2011+A1:2012. Madera estructural. Madera estructural y madera laminada. Determinación de algunas propiedades físicas y mecánicas (Spanish), (2012).
[31] Eos Systems Scanner. Vancouver BC, Canada. PhotoModeler Scanner (2018). https://www.photomodeler.com/products/scanner/ (accessed June 18, 2018).
[32] D. Naicu, R. Harris, C. Williams, Timber gridshells: Design methods and their application to a temporary pavilion, 2014.
[33] (Deleted to allow the required blind review).
[34] The Document Foundation, LibreOffice, (2014). https://www.libreoffice.org (accessed June 4, 2018).
[35] RibbonSoft GmbH, QCAD – 2D CAD for Windows, Linux and Mac, (2018). https://www.qcad.org/en (accessed May 16, 2018).
[36] C.S. Fraser, Innovations in automation for vision metrology systems, Photogramm. Rec. 15 (90) (1997) 901–911, https://doi.org/10.1111/0031-868X.00099.
[37] J. Zou, L. Meng, Design of a new coded target with large coding capacity for close-range photogrammetry and research on recognition algorithm, IEEE Access. 8 (2020) 220285–220292, https://doi.org/10.1109/ACCESS.2020.3043044.
[38] European Parliament and The Council of the EU, Directive 2014/32/EU of the European Parliament and of the Council of 26 February 2014 on the harmonisation of the laws of the Member States relating to the making available on the market of measuring instruments (recast), (2014). http://data.europa.eu/eli/dir/2014/32/2015-01-27.
[39] J.O. Sanz, M.d.l.L.G. Docampo, S.M. Rodríguez, M.T.R. Sanmartín, G.M. Cameselle, A simple methodology for recording petroglyphs using low-cost digital image correlation photogrammetry and consumer-grade digital cameras, J. Archaeol. Sci. 37 (12) (2010) 3158–3169.
[40] L. Liu, M. Sun, X. Ren, X. Liu, L. Liu, H. Zheng, X. Li, Review on methods of 3D reconstruction from uav image sequences, Beijing Daxue Xuebao (Ziran Kexue Ban)/Acta Sci Nat. Univ. Pekin. 53 (2017) 1165–1178. https://doi.org/10.13209/j.0479-8023.2017.052.
[41] M. Lieret, V. Kogan, C. Hofmann, J. Franke, Automated exploration, capture and photogrammetric reconstruction of interiors using an autonomous unmanned aircraft, in: 2021 IEEE Int. Conf. Mechatronics Autom. ICMA 2021, 2021: pp. 301–306. https://doi.org/10.1109/ICMA52036.2021.9512707.
[42] G. Caroti, A. Piemonte, I.M.-E. Zaragoza, G. Brambilla, Indoor photogrammetry using UAVs with protective structures: Issues and precision tests, in: Int. Arch. Photogramm. Remote Sens. Spat. Inf. Sci. - ISPRS Arch., 2018: pp. 137–142. https://doi.org/10.5194/isprs-archives-XLII-3-W4-137-2018.
[43] M. Casero, E. Covián, A. González, Regularization methods applied to noisy response from beams under static loading, J. Eng. Mech. 146 (6) (2020) 04020038, https://doi.org/10.1061/(ASCE)EM.1943-7889.0001765.